

# An Effective Model of Magnetoelectricity in Multiferroics $RMn_2O_5$

Chen Fang and Jiangping Hu

*Department of Physics, Purdue University, West Lafayette, Indiana 47907*

(Dated: April 22, 2017)

An effective model is developed to explain the phase diagram and the mechanism of magnetoelectric coupling in multiferroics,  $RMn_2O_5$ . We show that the nature of magnetoelectric coupling in  $RMn_2O_5$  is a coupling between two Ising-type orders, namely, the ferroelectric order in the  $b$  axis, and the coupled magnetic order between two frustrated antiferromagnetic chains. The frustrated magnetic structure drives the system to a commensurate-incommensurate phase transition, which can be understood as a competition between a collinear or col-plane order stemming from the ‘order by disorder’ mechanism and a chiral symmetry order. The low energy excitation is calculated and the effect of the external magnetic field is analyzed. Distinct features in the electromagnon spectrums in the incommensurate phase are predicted.

PACS numbers: 77.80.+q, 75.47.Lx, 77.80.-e

Recently, the search for new spin-electronics materials has led to a discovery of novel gigantic magnetoelectric and magnetocapacitive effects in rare-earth manganites, magnetoelectric multiferroics [1, 2]. Unlike the magnetic ferroelectrics studied in 1960s and 1970s where magnetism and ferroelectricity couple weakly, the magnetism and ferroelectricity in the new materials couple so strongly that the ferroelectricity can be easily manipulated by applying a magnetic field and the magnetic phase can be controlled by applying an electric field [3, 4]. This ease of manipulation promises great potential for important technological applications in novel spintronics devices.

The physics of the multiferroics involves the interplay between many degrees of freedom, such as charge, spin, orbital and lattice. Tremendous effort has been devoted to decode the fundamental mechanism of the strong coupling between the magnetism and ferroelectricity. Experimentally, two major classes of magnesium oxide multiferroics, have been discovered. The first class is the orthorhombic rare-earth manganites  $RMnO_3$  ( $R = Gd, Tb, Dy, \dots$ ) [5, 6], characterized by spiral magnetism strongly coupled with the ferroelectricity. An effective Ginzburg-Landau theory incorporating the space group symmetry and time reversal symmetry has been constructed to explain the fundamental physics [7]. Microscopically, Dzyaloshinskii-Moriya spin-orbit interaction is the underlying mechanism of the ferroelectricity [8, 9, 10]. The second class of materials are the manganese oxides with general formula  $RMn_2O_5$  ( $R = Y, Tb, Dy, \dots$ ) [11, 12, 13, 14]. These insulating materials consist of linked  $Mn^{4+}O_6$  octahedra and  $Mn^{3+}O_5$  pyramids with a  $Pbam$  space group symmetry. Unlike that in  $RMnO_3$ , the ferroelectricity in  $RMn_2O_5$  exists in a collinear or col-plane magnetic phase, suggesting that a different mechanism is involved in the interaction between the ferroelectricity and magnetism.

In this Letter, we develop an effective model to explain the phase diagram and the mechanism of magnetoelec-

tric coupling in  $RMn_2O_5$ . Building upon experimental facts and the space group symmetry [4, 11, 12, 13, 14, 15, 16, 17, 18, 19], we show that the magnetoelectric interaction is between two Ising type orders, the ferroelectric order in the  $b$  axis and the coupled magnetic order between two frustrated antiferromagnetic chains. The effective model of the magnetism can be derived from a microscopic model with nearest-neighbor magnetic exchange. We show that the effective model nicely captures the phase diagrams of  $RMn_2O_5$ . At high temperature, the commensurate (CM) collinear or col-plane order is stable due to the ‘order by disorder’ mechanism [20, 21, 22] and the existence of an easy axis. As the temperature decreases, a chiral symmetry order replaces the collinear or col-plane order, and the magnetic structure becomes incommensurate (ICM). This model predicts that an external magnetic field along the  $b$ -axis can drive the system from the ICM phase to the CM phase while that along the  $a$ -axis can drive the system from the CM phase to the ICM phase. The model predicts the following distinguished properties of low energy excitations: (1) the emergence of electromagnons in the ICM phase when there is no electromagnons at the lowest energy in the CM phase; (2) the presence of distinguished kinks in the energy dispersions of the electromagnons, unlike the dispersion of normal phason in conventional ICM phase which has a finite energy jump at the half of ICM wavevector [23]; (3) a double peak structure at low energy in optical conductivity due to the absorption of the electromagnons with a selection rule of the electric field along the  $b$  axis; (4) no new peak splitting in the electromagnon spectrums in the presence of external magnetic field along the  $a$  or  $b$  axis, which differs from the conventional picture of the Zeeman energy splitting of magnons; (5) the increase(decrease) of the energy gaps of the electromagnons as the field increases along the  $b(a)$  axis.

*Magnetoelectric coupling:* The ferroelectricity in  $RMn_2O_5$  is substantially different from that in  $RMnO_3$ .

Experiments have shown that the ferroelectricity only exists along the b axis in  $RMn_2O_5$ , but can be observed in both the a and c directions in  $RMnO_3$ . Most importantly, recent measurements of optical conductivity have revealed opposite selection rules for these two materials. In  $RMnO_3$ , low energy absorption is observed when the electric field is perpendicular to the static ferroelectric polarization direction[19, 24]. The opposite is true in  $RMn_2O_5$ , namely, low energy absorption is only observed when the electric field is polarized along the b axis[19]. This suggests that the electric degree of freedoms along the a and c axis simply has no coupling to magnetic degrees of freedom at low energy. Only the ferroelectricity along the b axis  $P_b$  couples to the magnetic degree of freedom. The order parameter  $P_b$  is an Ising-type order. Therefore, the nature of the magnetoelectric coupling in  $RMn_2O_5$  is a coupling between two Ising-type orders.( in the following paper, we refer the a,b,c axis to the x,y,z axis respectively for conveniences i.e.  $P_y = P_b$ ).

What is the Ising order in the magnetic side? The answer to this question can be obtained by in-depth analysis of the magnetic structure and the space group. As shown in [16, 17], the main magnetic structure along the a axis is two antiferromagnetic chains joined by  $Mn^{3+}$  and  $Mn^{4+}$  atoms (see Fig.1). The antiferromagnetic coupling between the two chains indicated by the red lines in Fig.1 are completely frustrated. Therefore, in an effective model, we at least need two antiferromagnetic orders  $\vec{n}_1$  and  $\vec{n}_2$  to describe the magnetic physics. A possible Ising order from these two vector magnetic orders is  $\vec{n}_1 \cdot \vec{n}_2$ . Due to the experiment fact that no magnetic moment in the c-axis is observed, it naturally leads to the construction of the possible lowest order magnetoelectric coupling between  $P_y$  and  $\vec{n}_i, i = 1, 2$  as

$$H_{em} = \lambda_x P_y n_1^x n_2^x + \lambda_y P_y n_1^y n_2^y \quad (1)$$

The possible differences between the coupling parameters  $\lambda_x$  and  $\lambda_y$  reflects real lattice structure.

Now we show that Eq.1 is consistent with the space group analysis. The space group of  $RMn_2O_5$  has been analyzed[25]. The lattice of  $RMn_2O_5$  belongs to Pbam structure. With the modulation vector  $q = (1/2, 0, k_c)$ , the space group has a single two dimensional irreducible representation in which the four symmetry lattice transforms can be represented by  $I, m_x = \sigma_x, m_y = \sigma_y, m_x m_y = i\sigma_z$  where  $\sigma_i$  are Pauli Matrix. Symmetry adapted variables can be constructed as linear combinations of spin operators that transform in accordance

with these matrices. The ion spins in one unit cell are numbered one to eight as shown in Fig.1. The space inversion symmetry, together with the experimental facts that  $S_1 = S_3, S_2 = S_4, S_5 = S_7, S_6 = -S_8$  and that the spin moments are only in a-b plane, suggests that the possibilities of magnetoelectric coupling term can be

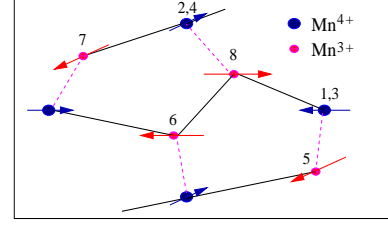


FIG. 1: A sketch of spin structures from a top view along the c axis in one unit cell of  $RMn_2O_5$ . The red lines reflect the frustrated magnetic coupling between two chains.

narrowed down to

$$H_{em} = i\lambda_x P_y (-S_2^x(q) S_6^{x*}(q) + S_1^x(q) S_5^{x*}(q) - c.c) + i\lambda_y P_y (-S_2^y(q) S_6^{y*}(q) + S_1^y(q) S_5^{y*}(q) - c.c). \quad (2)$$

Converting these spin operators to the two antiferromagnetic orders, we can simplify Eq.2 to Eq.1.

*Effective magnetic model:* In condensed matter physics, an effective model at low energy is largely independent of microscopic models if they share same essential physics. Therefore, one can derive the effective model on a much simplified lattice structure. In the case of  $RMn_2O_5$ , the important magnetic physics along the a axis are two antiferromagnetic chains with frustrated coupling[16, 17]. Experiments have shown a 1/4 commensurate magnetic wavevector along the c axis, which can also be viewed as an antiferromagnetic order if the unit cell is doubled along the c-axis. Therefore, we can derive the effective model from a microscopic model with two antiferromagnetic orders defined on the two interpenetrating sublattices as illustrated in Fig.2, where  $J_{1,(2)}$  are the effective antiferromagnetic exchange couplings which establish two antiferromagnetic orders,  $J_3$  is the effective frustrated coupling between two chains in one unit cell along the a axis and  $J_4$  is the effective frustrated coupling between two chains in two neighbor unit cells along the c axis. Using standard field theory[22, 26], we can show that the effective field theory described by the two antiferromagnetic orders  $\vec{n}_1$  and  $\vec{n}_2$  is given by the following Hamiltonian

$$H_m = \int \left\{ \sum_i \left[ \frac{\rho_{1s}}{2} (\partial n_i / \partial x)^2 + \frac{\rho_{2s}}{2} (\partial n_i / \partial z)^2 \right] + \alpha (n_1 \frac{\partial n_2}{\partial x} - n_2 \frac{\partial n_1}{\partial x}) - \right. \\ \left. \eta \left( \frac{\partial n_1}{\partial x} \frac{\partial n_2}{\partial z} + \frac{\partial n_1}{\partial z} \frac{\partial n_2}{\partial x} \right) - \tilde{g}(T) (n_1 \cdot n_2)^2 - D_0 \sum_i (n_i^x)^2 \right\} dx dz. \quad (3)$$

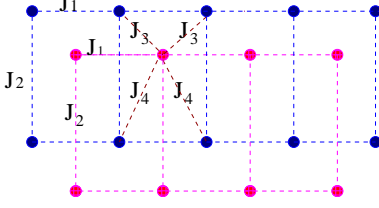


FIG. 2: A sketch of lattice structures of two frustrated coupled antiferromagnetic Heisenberg models in two dimension.

where  $\tilde{g}(T) = \tilde{g}_0 + \tilde{g}_1 T$  is a temperature dependent parameter induced by the quantum and thermal fluctuation, the parameter  $\alpha$  reflects that the intra frustrated coupling in one unit cell is larger than the inter frustrated coupling along the  $a$  axis between two neighbor unit cells along the  $c$  axis, and the parameter  $D_0$  describes a possible magnetic easy axis along the  $a$  axis. From the microscopic coupling parameter,  $\tilde{g}_1 = 0.26(J_1 + J_2)Sa^{-2}(\frac{J_3+J_4}{J_1+J_2})^2$ ,  $\tilde{g}_2 = 2.4\frac{\tilde{g}_1}{(J_1+J_2)S}$ ,  $\rho_{1s} = J_1 S^2$ ,  $\rho_{2s} = J_2 S^2$ ,  $\alpha = \frac{(J_1+J_2)S^2}{4} \frac{(J_3-J_4)}{(J_1+J_2)a}$  and  $\eta = \frac{(J_1+J_2)S^2}{4} \frac{J_3+J_4}{J_1+J_2}$ . Adding the lattice dynamics, we reach the total effective Hamiltonian as

$$H = \int dx dz \left[ \left( \frac{\kappa}{2} P_y^2 + \frac{1}{2M} \pi_y^2 \right) + H_{em} \right] + H_m \quad (4)$$

where  $\pi_y$  is the conjugate momentum of  $P_y$ .

The Hamiltonian in Eq.4 precisely captures the phase diagrams of  $RMn_2O_5$ [4, 11, 15]. To study the magnetic phase diagram, we can integrate out the lattice dynamics. After integrating out the lattice dynamics, the effective magnetic Hamiltonian is the Hamiltonian in Eq.10 with a replacement of  $\tilde{g}$  by  $g(T) = g_0 + \tilde{g}_1 T$  where  $g_0 = \tilde{g}_0 + \frac{\lambda_\pm^2}{8\kappa}$ ,  $D_0$  by  $D = D_0 + \frac{\lambda_\pm \lambda_\mp}{4\kappa}$  and an additional term  $-\gamma(n_1^x n_2^x - n_1^y n_2^y)^2$  where  $\gamma = \frac{\lambda_\pm^2}{8\kappa}$  and  $\lambda_\pm = \lambda_x \pm \lambda_y$ . It is clear that the  $\alpha$  term favors an ICM phase while  $g(T)$ ,  $\gamma$  and  $D$  favor a CM phase. If  $D \neq 0$ , at relatively high transition temperature  $T_{c1}$ , the model exhibits a first phase transition to a collinear magnetic phase with order  $\langle n_1^x n_2^x \rangle \neq 0$  and then exhibits a second phase transition at  $T_{c2} < T_{c1}$  with order  $\langle n_1^y n_2^y \rangle \neq 0$ . The collinear phase becomes a col-plane phase. The ferroelectricity is given by  $\langle P_y \rangle = -\frac{\lambda_x \langle n_1^x n_2^x \rangle + \lambda_y \langle n_1^y n_2^y \rangle}{\kappa}$ . With the proper values of  $\alpha$ , at a low temperature  $T_{IC}$ , the ICM phase can win over the col-plane magnetic phase.

In the ICM phase, the global average,  $\langle P_y \rangle = 0$ . Fig.3 sketches the phase diagram. The phase diagram qualitatively matches the current experimental results on the phase diagram of  $RMn_2O_5$ [4, 11, 15]. Results from mean field or large  $N$  limit calculation, using the real experimental data as input, will be reported elsewhere[27]. In this paper, we present a thorough study of the simplified version of the model in one dimension which captures the essential low energy physics.

*Coupled Sine-Gordon model:* We focus on an one-dimensional effective model by ignoring the dynamics in  $z$  direction in Eq.4. The one dimensional model still captures essential physics of the frustration. For the one dimensional model, we can go beyond mean field calculation and evaluate the dynamics in a controllable perturbation manner. Using the angle to parameterize the antiferromagnetic vector in  $x$ - $y$  plane as  $\vec{n}_i = (\cos\theta_i, \sin\theta_i)$ , we obtain the effective Hamiltonian in one dimension as a coupled Sine-Gordon model,

$$H = \frac{\rho}{2} \left( \frac{\partial \theta_-}{\partial x} \right)^2 + \alpha \sin \theta_- \frac{\partial \theta_+}{\partial x} - g \cos^2 \theta_- - \gamma \cos^2 \theta_+ \\ + \frac{\rho}{2} \left( \frac{\partial \theta_+}{\partial x} \right)^2 - D \cos \theta_+ \cos \theta_-, \quad (5)$$

where  $\theta_\pm = \theta_1 \pm \theta_2$ . Minimizing the potential part in Eq.5, the CM-ICM phase transition line is estimated to be

$$\rho(g(T) + \gamma/2 + D) = \alpha^2/2 + \frac{D^2}{2(\alpha^2 - \rho g(T))}. \quad (6)$$

To obtain a more accurate result, we can apply a controllable numerical method[28]. In the CM phase, the ground state of the model is always described by  $\theta_+ = \theta_- = 0$  or  $\pi$ . In the ICM phase, it is clear that the spins on the two antiferromagnetic chains are both rotating with the same wave vector  $q$  throughout the system. Therefore, we can take the following ansatz:  $\theta_-(x) = \sum_{n=0}^{\infty} (a_n \cos nqx + b_n \sin nqx)$  and  $\theta_+(x) = qx + \sum_{n=0}^{\infty} (c_n \cos nqx + d_n \sin nqx)$ . The coefficient in this ansatz decreases rapidly as  $n$  increases. As an example, for a typical set of parameters  $\{\rho = 2, \alpha = 0.4, g = 0.03, \gamma = 0.01, d = 0.005\}$ , a numerical solution of the ICM ground state is given by  $\theta_+ = qx + 0.0322 \sin(2qx) - 0.000255 \sin(4qx) + \dots$  and  $\theta_- = -\frac{\pi}{2} + 0.0526 \cos(qx) + 0.0000676 \cos(3qx) + \dots$ , where  $q = 0.199$ . Therefore, the first two terms in the ansatz

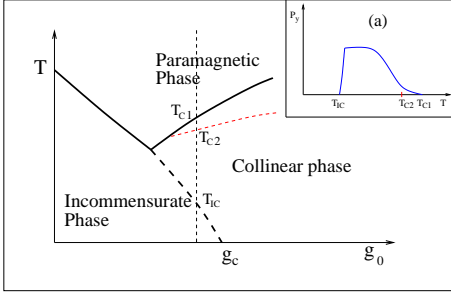


FIG. 3: The phase diagram as  $g_0$  vs  $T$ . The vertical dashed line represents phase transitions in most of  $RMn_2O_5$  materials. The inset (a) is the ferroelectricity as a function of temperature.

can give us a very good approximation of the ground state.

*Energy dispersion of magnons in the CM phase:* In the CM phase, the ferroelectricity,  $\langle P_y \rangle = -\frac{\lambda_+ + \lambda_-}{2\kappa}$ . The dynamics of magnons and the dynamics of electric degree of freedoms are decoupled. To show this, one can expand the free energy at the vicinity of the ground state,  $u_1 = \delta\theta_+$ ,  $u_2 = \delta\theta_-$ ,  $\beta = \delta P_y$  and show that there is no second order coupling between  $u_i$  and  $\beta$  (the lowest order coupling between  $u_i$  and  $\beta$  is  $\lambda_+ \beta u_2^2 + \lambda_- \beta u_1^2$ ). Therefore, there is no electromagnon excitation. The energy dispersions of the two magnons in the CM phase are given by

$$E_{cm}^{\pm} = \sqrt{\rho(\rho k^2 + \gamma + g + D \pm \sqrt{(g - \gamma)^2 + \alpha^2 k^2})}. \quad (7)$$

*Electromagnons in the ICM phase:* In the ICM phase,  $\langle P_y(x) \rangle = -\frac{\lambda_+}{2\kappa} \cos(qx)$  where  $q$  is the ICM wavevector. The magnon and phonon dynamics are coupled due to the ICM modulation. Therefore, the low energy excitations are electromagnons. To calculate the dispersion, we expand the Hamiltonian at the vicinity of the ICM phase,  $u_1 = \delta\theta_+$ ,  $u_2 = \delta\theta_-$  and  $\beta = \delta P_y$ . The fluctuation up to the second order of these dynamic variables is given by  $\delta H^{(2)} = \delta H_0^{(2)} + \delta H_1^{(2)}$ . The first term is the free part given by

$$\delta H_0^{(2)} = \sum_k \left( \sum_{i=1}^2 E_i(k) \mu_i(k) \mu_i(-k) + \omega_0^2 \beta(k) \beta(-k) \right) \quad (8)$$

with  $E_1(k) = \rho k^2 + \frac{Da_+}{2} + \frac{\lambda_-(a_1 \lambda + \lambda_-)}{4\kappa}$ ,  $E_2(k) = E_1(k) + \Delta_0$  where  $\Delta_0 = \alpha q - 2\tilde{g} - \frac{\lambda_-^2}{4\kappa}$  and the phonon frequency  $\omega_0 = \sqrt{\kappa}$  (for convenience, we have taken the mass  $M = 1$  in Eq.4). The second term is the interaction part

$$\begin{aligned} \delta H_1^{(2)} = & \int dx [\alpha a_1 \cos(qx) u_1' u_2 + D \sin(qx) u_1 u_2 \\ & + \frac{1}{2} \beta (-\lambda_- u_1 \sin(qx) + \lambda_+ u_2)]. \end{aligned} \quad (9)$$

In Eq.9, the terms in the first line couple  $u_1(k)$  with  $u_2(k \pm q)$  and vice versa and modify the gap  $\Delta_0$  between

two magnon modes. In general, as shown in Fig.4, the coupling creates a distinguished kink in dispersion curve around  $k = q/2$  rather than a finite energy jump at  $k = q/2$  which is normally expected in the ICM phase described in a simple Sine-Gordon model[23]. The terms in the second line describe the coupling between the magnon and the phonon. The coupling results in two general effects. First, the coupling leads to a change of phonon frequency. Under condition  $\omega_0^2 \gg \rho E_i(0)$ , the shift frequency of the phonon is roughly given by  $\delta\omega^2 = \frac{\rho\lambda_+^2}{4(\omega_0^2 - \rho E_2(0))} + \frac{\rho\lambda_-^2}{8(\omega_0^2 - \rho E_2(q))}$ . Second, the coupling allows us to measure the magnons in optical conductivity. The optical conductivity is given by  $\sigma(\omega) = \omega \text{Im}[G_{\beta\beta}(\omega, 0)]$ , where  $G_{\beta\beta}(\omega, k)$  is the full propagator of the  $\beta$ . In our model, we expect double peaks in the optical conductivity at the gap energy of the two magnons in the ICM phase. Up to the second order, we have,  $\text{Im}[G_{\beta\beta}(\omega, 0)] = \pi [\rho \frac{\lambda_-^2}{8\omega_0^4} \delta(\omega^2 - \rho E_1(q)) + \rho \frac{\lambda_+^2}{4\omega_0^4} \delta(\omega^2 - \rho E_2(0)) + (1 - \rho \frac{\lambda_-^2/2 + \lambda_+^2}{4\omega_0^4}) \delta(\omega^2 - \omega_0^2 - \delta\omega^2)]$ . In Fig.4, by numerically solving the dynamical equations of  $\delta H^{(2)}$ , we plot the result of  $\sigma(\omega)$  and the dispersions of electromagnons with a typical parameter setting  $\{\rho, \alpha, \lambda_+, \lambda_-, \kappa, D, g\} = \{2, 0.4, 0.06, 0.06, 2, 0.002, 0.005\}$ .

*Effects of external magnetic field:* In our model, since  $\vec{n}$  is the staggered moment field, the effect of an external magnetic field  $H$  is equivalent to creating an easy plane. However, since the staggered moment is in the a-b plane, the effect of the field is only important when the field is along the a or b axis. In the presence of the easy axis parameter  $D$  along the a axis, the effects of the external magnetic fields along the a axis,  $H_a$ , and b axis,  $H_b$ , have exact opposite effects. They simply change  $D$  to

$$D(H_a, H_b) = D - H_a^2/2\rho + H_b^2/2\rho \quad (10)$$

in Eq.5. From  $E_1(k)$ ,  $E_2(k)$ , Eq.9 and Eq.6, Eq.10 leads to a few important and immediate predictions. First, the effects of  $H_a$  and  $H_b$  do not depend on their directions along their own axis. Second,  $H_b$  can drive the system from the ICM phase to the CM phase while  $H_a$  can drive the system from the CM phase to the ICM phase. This result has been observed experimentally in [12]. The critical fields to drive the transition can be estimated for the one dimensional system from Eq.6. Third, in the ICM phase, the energy dispersions of the electromagnons as a function of  $H_a$  and  $H_b$  can be predicted. From  $E_1(k)$ ,  $E_2(k)$  and Eq.9, the energy of the electromagnons is expected to increase (decrease) as  $H_b$  ( $H_a$ ) increases. Finally, the external magnetic field does not add additional peaks, which contradicts the conventional picture of the Zeeman energy splitting of magnons.

In conclusion, we develop an effective model that explains the phase diagram and the mechanism of magnetoelectric coupling in multiferroics  $RMn_2O_5$ . To our knowledge, this is the first theoretical effective model

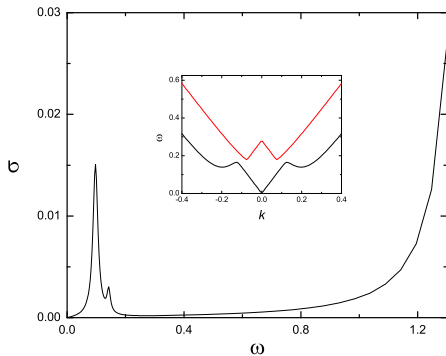


FIG. 4: The numerical result of the optical conductivity versus frequency with the parameters set to:  $\{\rho, \alpha, \lambda_+, \lambda_-, \kappa, D, g\} = \{2, 0.4, 0.06, 0.06, 2, 0.002, 0.005\}$ . The inset is the dispersion of the electromagnons.

for these materials. A detailed study of low energy excitations in one dimension is performed to explain the selection rules of electromagnon in optical conductivity measurements[19]. Our prediction of the electromagnon dispersion and its dependence on the external magnetic field can be tested in future experiments. A quantitative study of our model incorporating the experimental data on different  $RMn_2O_5$  materials will be reported elsewhere[27]. We expect that the model presented here can be applied to other multiferronics materials where ferroelectricity is correlated to a collinear or col-plane magnetic phase.

*Acknowledgments* J. Hu thanks S. Kivelson and S. Brown for teaching some concepts presented in this paper. We thank A. B. Sushkov, R.V. Aguilar and D. Drew for important comments and extremely useful discussion. We also thank M. Mostovoy for useful discussion in APS March meeting (2007). This work was supported by the National Science Foundation under grant number PHY-0603759.

[1] Y. Tokura, Science **312**, 1481 (2006).

[2] S. W. Cheong and M. Mostovoy, Nature Materials **6**, 13 (2007).

- [3] T. Kimura, T. Goto, H. Shintani, K. Ishizaka, T. Arima, and Y. Tokura, Nature **426**, 55 (2003).
- [4] N. Hur, S. Park, P. A. Sharma, J. S. Ahn, S. Guha, and S. W. Cheong, Nature **429**, 392 (2004).
- [5] T. Kimura, S. Kawamoto, I. Yamada, M. Azuma, M. Takano, and Y. Tokura, Phys. Rev. B **67**, 180401 (2003).
- [6] T. Goto, T. Kimura, G. Lawes, A. P. Ramirez, and Y. Tokura, Phys. Rev. Lett. **92**, 257201 (2004).
- [7] M. Mostovoy, Phys. Rev. Lett. **96**, 067601 (2006).
- [8] H. Katsura, N. Nagaosa, and A. V. Balatsky, Phys. Rev. Lett. **95**, 057205 (2005).
- [9] H. Katsura, A. V. Balatsky, and N. Nagaosa, Phys. Rev. Lett. **98**, 027203 (2007).
- [10] I. A. Sergienko and E. Dagotto, Phys. Rev. B **73**, 094434 (2006).
- [11] I. Kigomiya, S. Matsumoto, K. Kohn, Y. Fukuda, T. Shoubu, H. Kimura, Y. Noda, and N. Ikeda, Ferroelectrics **286**, 167 (2003).
- [12] N. Hur, S. Park, P. A. Sharma, S. Guha, and S. W. Cheong, Phys. Rev. Lett. **93**, 107207 (2004).
- [13] L. C. Chapon, G. R. Blake, M. J. Gutmann, S. Park, N. Hur, P. G. Radaelli, and S. W. Cheong, Phys. Rev. Lett. **93**, 177402 (2004).
- [14] A. M. Kadomtseva, S. S. Krotov, Y. F. Popov, and G. P. Vorob'ev, Low Temp. Phys. **32**, 709 (2006).
- [15] L. C. Chapon, G. R. Blake, a. S. P. M. J. Gutmann, N. Hur, P. G. Radaelli, and S.-W. Cheong, Phys. Rev. Lett. **93**, 177402 (2004).
- [16] L. C. Chapon, P. G. Radaelli, G. R. Blake, S. Park, and S.-W. Cheong, Phys. Rev. Lett. **96**, 097601 (2006).
- [17] G. R. Blake, L. C. Chapon, P. G. Radaelli, S. Park, N. Hur, S.-W. Cheong, and J. Rodriguez-Carvajal, Phys. Rev. B **71**, 214402 (2005).
- [18] I. Radulov, V. Lovchinov, and M. Daszkiewicz, cond-mat p. 0701687 (2007).
- [19] A. B. Sushkov, R. V. Aguilar, S. Park, S.-W. Cheong, and H. D. Drew, Phys. Rev. Lett. **98**, 027202 (2007).
- [20] E. F. Shender, Sov. Phys. JEPT **56**, 178 (1982).
- [21] A. L. P. Chandra, P. Coleman, Phys. Rev. Lett. **64**, 88 (1990).
- [22] C. L. Henley, Phys. Rev. Lett. **62**, 2056 (1989).
- [23] P. Bak, Rep. Prog. Phys. **45**, 587 (1982).
- [24] A. Pimenov, A. A. Mukhin, V. Y. Ivanov, V. D. Travkin, A. M. Balbashov, and A. Loidl, Nature Physics **2**, 97 (2006).
- [25] A. B. Harris, cond-mat/0610241 (2006).
- [26] A. M. Tsvelik, "Quantum Field Theory in condensed matter physics", published by Cambridge Univ. Press, (2003).
- [27] C. Fang and J. Hu, to be published (2007).
- [28] W. L. McMillan, Phys. Rev. B **12**, 2042 (1975).

# An Effective Model of Magnetoelectricity in Multiferroics $RMn_2O_5$

Chen Fang<sup>1</sup> and Jiangping Hu<sup>1</sup>

<sup>1</sup>*Department of Physics, Purdue University, West Lafayette, Indiana 47907*

(Dated: April 22, 2017)

An effective model is developed to explain the phase diagram and the mechanism of magnetoelectric coupling in multiferroics,  $RMn_2O_5$ . We show that the nature of magnetoelectric coupling in  $RMn_2O_5$  is a coupling between two Ising-type orders, namely, the ferroelectric order in the b axis, and the coupled magnetic order between two frustrated antiferromagnetic chains. The frustrated magnetic structure drives the system to a commensurate-incommensurate phase transition, which can be understood as a competition between a collinear or col-plane order stemming from the ‘order by disorder’ mechanism and a chiral symmetry order. The low energy excitation is calculated and the effect of the external magnetic field is analyzed. Distinct features in the electromagnon spectrums in the incommensurate phase are predicted.

PACS numbers: 77.80.+q, 75.47.Lx, 77.80.-e

Recently, the search for new spin-electronics materials has led to a discovery of novel gigantic magnetoelectric and magnetocapacitive effects in rare-earth manganites, magnetoelectric multiferroics [? ? ]. Unlike the magnetic ferroelectrics studied in 1960s and 1970s where magnetism and ferroelectricity couple weakly, the magnetism and ferroelectricity in the new materials couple so strongly that the ferroelectricity can be easily manipulated by applying a magnetic field and the magnetic phase can be controlled by applying an electric field [? ? ]. This ease of manipulation promises great potential for important technological applications in novel spintronics devices.

The physics of the multiferroics involves the interplay between many degrees of freedom, such as charge, spin, orbital and lattice. Tremendous effort has been devoted to decode the fundamental mechanism of the strong coupling between the magnetism and ferroelectricity. Experimentally, two major classes of magnesium oxide multiferroics, have been discovered. The first class is the orthorhombic rare-earth manganites  $RMnO_3$  ( $R = Gd, Tb, Dy, \dots$ ) [? ? ], characterized by spiral magnetism strongly coupled with the ferroelectricity. An effective Ginzburg-Landau theory incorporating the space group symmetry and time reversal symmetry has been constructed to explain the fundamental physics [? ]. Microscopically, Dzyaloshinskii-Moriya spin-orbit interaction is the underlying mechanism of the ferroelectricity [? ? ? ]. The second class of materials are the manganese oxides with general formula  $RMn_2O_5$  ( $R = Y, Tb, Dy, \dots$ ) [? ? ? ? ]. These insulating materials consist of linked  $Mn^{4+}O_6$  octahedra and  $Mn^{3+}O_5$  pyramids with a  $Pbam$  space group symmetry. Unlike that in  $RMnO_3$ , the ferroelectricity in  $RMn_2O_5$  exists in a collinear or col-plane magnetic phase, suggesting that a different mechanism is involved in the interaction between the ferroelectricity and magnetism.

In this Letter, we develop an effective model to explain the phase diagram and the mechanism of magnetoelec-

tric coupling in  $RMn_2O_5$ . Building upon experimental facts and the space group symmetry [? ? ? ? ? ? ? ? ], we show that the magnetoelectric interaction is between two Ising type orders, the ferroelectric order in the b axis and the coupled magnetic order between two frustrated antiferromagnetic chains. The effective model of the magnetism can be derived from a microscopic model with nearest-neighbor magnetic exchange. We show that the effective model nicely captures the phase diagrams of  $RMn_2O_5$ . At high temperature, the commensurate (CM) collinear or col-plane order is stable due to the ‘order by disorder’ mechanism [? ? ? ] and the existence of an easy axis. As the temperature decreases, a chiral symmetry order replaces the collinear or col-plane order, and the magnetic structure becomes incommensurate (ICM). This model predicts that an external magnetic field along the b-axis can drive the system from the ICM phase to the CM phase while that along the a-axis can drive the system from the CM phase to the ICM phase. The model predicts the following distinguished properties of low energy excitations: (1) the emergence of electromagnons in the ICM phase when there is no electromagnons at the lowest energy in the CM phase; (2) the presence of distinguished kinks in the energy dispersions of the electromagnons, unlike the dispersion of normal phason in conventional ICM phase which has a finite energy jump at the half of ICM wavevector [? ]; (3) a double peak structure at low energy in optical conductivity due to the absorption of the electromagnons with a selection rule of the electric field along the b axis; (4) no new peak splitting in the electromagnon spectrums in the presence of external magnetic field along the a or b axis, which differs from the conventional picture of the Zeeman energy splitting of magnons; (5) the increase(decrease) of the energy gaps of the electromagnons as the field increases along the b(a) axis.

*Magnetoelectric coupling:* The ferroelectricity in  $RMn_2O_5$  is substantially different from that in  $RMnO_3$ . Experiments have shown that the ferroelectricity only ex-



ists along the b axis in  $RMn_2O_5$ , but can be observed in both the a and c directions in  $RMnO_3$ . Most importantly, recent measurements of optical conductivity have revealed opposite selection rules for these two materials. In  $RMnO_3$ , low energy absorption is observed when the electric field is perpendicular to the static ferroelectric polarization direction[? ? ]. The opposite is true in  $RMn_2O_5$ , namely, low energy absorption is only observed when the electric field is polarized along the b axis[? ]. This suggests that the electric degree of freedoms along the a and c axis simply has no coupling to magnetic degrees of freedom at low energy. Only the ferroelectricity along the b axis  $P_b$  couples to the magnetic degree of freedom. The order parameter  $P_b$  is an Ising-type order. Therefore, the nature of the magnetoelectric coupling in  $RMn_2O_5$  is a coupling between two Ising-type orders.( in the following paper, we refer the a,b,c axis to the x,y,z axis respectively for conveniences i.e.  $P_y = P_b$ ).

What is the Ising order in the magnetic side? The answer to this question can be obtained by in-depth analysis of the magnetic structure and the space group. As shown in [? ? ],the main magnetic structure along the a axis is two antiferromagnetic chains joined by  $Mn^{3+}$  and  $Mn^{4+}$  atoms (see Fig.1). The antiferromagnetic coupling between the two chains indicated by the red lines in Fig.1 are completely frustrated. Therefore, in an effective model, we at least need two antiferromagnetic orders  $\vec{n}_1$  and  $\vec{n}_2$  to describe the magnetic physics. A possible Ising order from these two vector magnetic orders is  $\vec{n}_1 \cdot \vec{n}_2$ . Due to the experiment fact that no magnetic moment in the c-axis is observed, it naturally leads to the construction of the possible lowest order magnetoelectric coupling between  $P_y$  and  $\vec{n}_i, i = 1, 2$  as

$$H_{em} = \lambda_x P_y n_1^x n_2^x + \lambda_y P_y n_1^y n_2^y \quad (1)$$

The possible differences between the coupling parameters  $\lambda_x$  and  $\lambda_y$  reflects real lattice structure.

Now we show that Eq.1 is consistent with the space group analysis. The space group of  $RMn_2O_5$  has been analyzed[? ]. The lattice of  $RMn_2O_5$  belongs to Pbam structure. With the modulation vector  $q = (1/2, 0, k_c)$ , the space group has a single two dimensional irreducible representation in which the four symmetry lattice transforms can be represented by  $I, m_x = \sigma_x, m_y = \sigma_y, m_x m_y = i\sigma_z$  where  $\sigma_i$  are Pauli Matrix. Symmetry adapted variables can be constructed as linear combinations of spin operators that transform in accordance

with these matrices. The ion spins in one unit cell are numbered one to eight as shown in Fig.1. The space inversion symmetry, together with the experimental facts that  $S_1 = S_3, S_2 = S_4, S_5 = S_7, S_6 = -S_8$  and that the spin moments are only in a-b plane, suggests that the possibilities of magnetoelectric coupling term can be

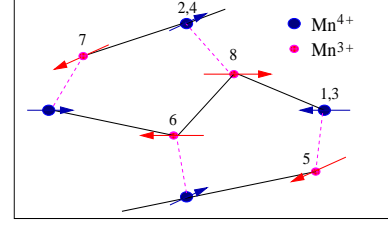


FIG. 1: A sketch of spin structures from a top view along the c axis in one unit cell of  $RMn_2O_5$ . The red lines reflect the frustrated magnetic coupling between two chains.

narrowed down to

$$H_{em} = i\lambda_x P_y (-S_2^x(q) S_6^{x*}(q) + S_1^x(q) S_5^{x*}(q) - c.c) + i\lambda_y P_y (-S_2^y(q) S_6^{y*}(q) + S_1^y(q) S_5^{y*}(q) - c.c). \quad (2)$$

Converting these spin operators to the two antiferromagnetic orders, we can simplify Eq.2 to Eq.1.

*Effective magnetic model:* In condensed matter physics, an effective model at low energy is largely independent of microscopic models if they share same essential physics. Therefore, one can derive the effective model on a much simplified lattice structure. In the case of  $RMn_2O_5$ , the important magnetic physics along the a axis are two antiferromagnetic chains with frustrated coupling[? ? ]. Experiments have shown a 1/4 commensurate magnetic wavevector along the c axis, which can also be viewed as an antiferromagnetic order if the unit cell is doubled along the c-axis. Therefore, we can derive the effective model from a microscopic model with two antiferromagnetic orders defined on the two interpenetrating sublattices as illustrated in Fig.2, where  $J_{1,(2)}$  are the effective antiferromagnetic exchange couplings which establish two antiferromagnetic orders,  $J_3$  is the effective frustrated coupling between two chains in one unit cell along the a axis and  $J_4$  is the effective frustrated coupling between two chains in two neighbor unit cells along the c axis. Using standard field theory[? ? ], we can show that the effective field theory described by the two antiferromagnetic orders  $\vec{n}_1$  and  $\vec{n}_2$  is given by the following Hamiltonian

$$H_m = \int \left\{ \sum_i \left[ \frac{\rho_{1s}}{2} (\partial n_i / \partial x)^2 + \frac{\rho_{2s}}{2} (\partial n_i / \partial z)^2 \right] + \alpha (n_1 \frac{\partial n_2}{\partial x} - n_2 \frac{\partial n_1}{\partial x}) - \right. \\ \left. \eta \left( \frac{\partial n_1}{\partial x} \frac{\partial n_2}{\partial z} + \frac{\partial n_1}{\partial z} \frac{\partial n_2}{\partial x} \right) - \tilde{g}(T) (n_1 \cdot n_2)^2 - D_0 \sum_i (n_i^x)^2 \right\} dx dz. \quad (3)$$

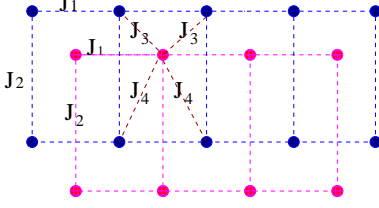


FIG. 2: A sketch of lattice structures of two frustrated coupled antiferromagnetic Heisenberg models in two dimension.

where  $\tilde{g}(T) = \tilde{g}_0 + \tilde{g}_1 T$  is a temperature dependent parameter induced by the quantum and thermal fluctuation, the parameter  $\alpha$  reflects that the intra frustrated coupling in one unit cell is larger than the inter frustrated coupling along the  $a$  axis between two neighbor unit cells along the  $c$  axis, and the parameter  $D_0$  describes a possible magnetic easy axis along the  $a$  axis. From the microscopic coupling parameter,  $\tilde{g}_1 = 0.26(J_1 + J_2)Sa^{-2}(\frac{J_3+J_4}{J_1+J_2})^2$ ,  $\tilde{g}_2 = 2.4\frac{\tilde{g}_1}{(J_1+J_2)S}$ ,  $\rho_{1s} = J_1 S^2$ ,  $\rho_{2s} = J_2 S^2$ ,  $\alpha = \frac{(J_1+J_2)S^2}{4} \frac{(J_3-J_4)}{(J_1+J_2)a}$  and  $\eta = \frac{(J_1+J_2)S^2}{4} \frac{J_3+J_4}{J_1+J_2}$ . Adding the lattice dynamics, we reach the total effective Hamiltonian as

$$H = \int dx dz \left[ \left( \frac{\kappa}{2} P_y^2 + \frac{1}{2M} \pi_y^2 \right) + H_{em} \right] + H_m \quad (4)$$

where  $\pi_y$  is the conjugate momentum of  $P_y$ .

The Hamiltonian in Eq.4 precisely captures the phase diagrams of  $RMn_2O_5$ [? ? ?]. To study the magnetic phase diagram, we can integrate out the lattice dynamics. After integrating out the lattice dynamics, the effective magnetic Hamiltonian is the Hamiltonian in Eq.10 with a replacement of  $\tilde{g}$  by  $g(T) = g_0 + \tilde{g}_1 T$  where  $g_0 = \tilde{g}_0 + \frac{\lambda_{\pm}^2}{8\kappa}$ ,  $D_0$  by  $D = D_0 + \frac{\lambda_{\pm}\lambda_{\mp}}{4\kappa}$  and an additional term  $-\gamma(n_1^x n_2^x - n_1^y n_2^y)^2$  where  $\gamma = \frac{\lambda_{\pm}^2}{8\kappa}$  and  $\lambda_{\pm} = \lambda_x \pm \lambda_y$ . It is clear that the  $\alpha$  term favors an ICM phase while  $g(T)$ ,  $\gamma$  and  $D$  favor a CM phase. If  $D \neq 0$ , at relatively high transition temperature  $T_{c1}$ , the model exhibits a first phase transition to a collinear magnetic phase with order  $\langle n_1^x n_2^x \rangle \neq 0$  and then exhibits a second phase transition at  $T_{c2} < T_{c1}$  with order  $\langle n_1^y n_2^y \rangle \neq 0$ . The collinear phase becomes a col-plane phase. The ferroelectricity is given by  $\langle P_y \rangle = -\frac{\lambda_x \langle n_1^x n_2^x \rangle + \lambda_y \langle n_1^y n_2^y \rangle}{\kappa}$ . With the proper values of  $\alpha$ , at a low temperature  $T_{IC}$ , the ICM phase can win over the col-plane magnetic phase.

In the ICM phase, the global average,  $\langle P_y \rangle = 0$ . Fig.3 sketches the phase diagram. The phase diagram qualitatively matches the current experimental results on the phase diagram of  $RMn_2O_5$ [? ? ?]. Results from mean field or large  $N$  limit calculation, using the real experimental data as input, will be reported elsewhere[?]. In this paper, we present a thorough study of the simplified version of the model in one dimension which captures the essential low energy physics.

*Coupled Sine-Gordon model:* We focus on an one-dimensional effective model by ignoring the dynamics in  $z$  direction in Eq.4. The one dimensional model still captures essential physics of the frustration. For the one dimensional model, we can go beyond mean field calculation and evaluate the dynamics in a controllable perturbation manner. Using the angle to parameterize the antiferromagnetic vector in  $x$ - $y$  plane as  $\vec{n}_i = (\cos\theta_i, \sin\theta_i)$ , we obtain the effective Hamiltonian in one dimension as a coupled Sine-Gordon model,

$$H = \frac{\rho}{2} \left( \frac{\partial \theta_-}{\partial x} \right)^2 + \alpha \sin \theta_- \frac{\partial \theta_+}{\partial x} - g \cos^2 \theta_- - \gamma \cos^2 \theta_+ \\ + \frac{\rho}{2} \left( \frac{\partial \theta_+}{\partial x} \right)^2 - D \cos \theta_+ \cos \theta_-, \quad (5)$$

where  $\theta_{\pm} = \theta_1 \pm \theta_2$ . Minimizing the potential part in Eq.5, the CM-ICM phase transition line is estimated to be

$$\rho(g(T) + \gamma/2 + D) = \alpha^2/2 + \frac{D^2}{2(\alpha^2 - \rho g(T))}. \quad (6)$$

To obtain a more accurate result, we can apply a controllable numerical method[?]. In the CM phase, the ground state of the model is always described by  $\theta_+ = \theta_- = 0$  or  $\pi$ . In the ICM phase, it is clear that the spins on the two antiferromagnetic chains are both rotating with the same wave vector  $q$  throughout the system. Therefore, we can take the following ansatz:  $\theta_-(x) = \sum_{n=0}^{\infty} (a_n \cos nqx + b_n \sin nqx)$  and  $\theta_+(x) = qx + \sum_{n=0}^{\infty} (c_n \cos nqx + d_n \sin nqx)$ . The coefficient in this ansatz decreases rapidly as  $n$  increases. As an example, for a typical set of parameters  $\{\rho = 2, \alpha = 0.4, g = 0.03, \gamma = 0.01, d = 0.005\}$ , a numerical solution of the ICM ground state is given by  $\theta_+ = qx + 0.0322 \sin(2qx) - 0.000255 \sin(4qx) + \dots$  and  $\theta_- = -\frac{\pi}{2} + 0.0526 \cos(qx) + 0.0000676 \cos(3qx) + \dots$ , where  $q = 0.199$ . Therefore, the first two terms in the ansatz



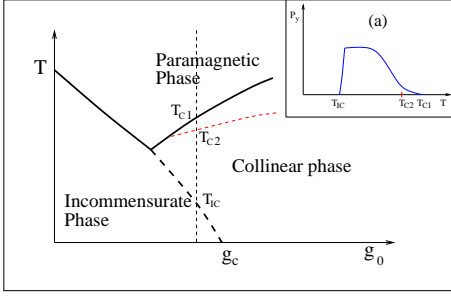


FIG. 3: The phase diagram as  $g_0$  vs  $T$ . The vertical dashed line represents phase transitions in most of  $RMn_2O_5$  materials. The inset (a) is the ferroelectricity as a function of temperature.

can give us a very good approximation of the ground state.

*Energy dispersion of magnons in the CM phase:* In the CM phase, the ferroelectricity,  $\langle P_y \rangle = -\frac{\lambda_+ + \lambda_-}{2\kappa}$ . The dynamics of magnons and the dynamics of electric degree of freedoms are decoupled. To show this, one can expand the free energy at the vicinity of the ground state,  $u_1 = \delta\theta_+$ ,  $u_2 = \delta\theta_-$ ,  $\beta = \delta P_y$  and show that there is no second order coupling between  $u_i$  and  $\beta$  (the lowest order coupling between  $u_i$  and  $\beta$  is  $\lambda_+ \beta u_2^2 + \lambda_- \beta u_1^2$ ). Therefore, there is no electromagnon excitation. The energy dispersions of the two magnons in the CM phase are given by

$$E_{cm}^{\pm} = \sqrt{\rho(\rho k^2 + \gamma + g + D \pm \sqrt{(g - \gamma)^2 + \alpha^2 k^2})}. \quad (7)$$

*Electromagnons in the ICM phase:* In the ICM phase,  $\langle P_y(x) \rangle = -\frac{\lambda_+}{2\kappa} \cos(qx)$  where  $q$  is the ICM wavevector. The magnon and phonon dynamics are coupled due to the ICM modulation. Therefore, the low energy excitations are electromagnons. To calculate the dispersion, we expand the Hamiltonian at the vicinity of the ICM phase,  $u_1 = \delta\theta_+$ ,  $u_2 = \delta\theta_-$  and  $\beta = \delta P_y$ . The fluctuation up to the second order of these dynamic variables is given by  $\delta H^{(2)} = \delta H_0^{(2)} + \delta H_1^{(2)}$ . The first term is the free part given by

$$\delta H_0^{(2)} = \sum_k \left( \sum_{i=1}^2 E_i(k) \mu_i(k) \mu_i(-k) + \omega_0^2 \beta(k) \beta(-k) \right) \quad (8)$$

with  $E_1(k) = \rho k^2 + \frac{Da_+}{2} + \frac{\lambda_-(a_1 \lambda_+ + \lambda_-)}{4\kappa}$ ,  $E_2(k) = E_1(k) + \Delta_0$  where  $\Delta_0 = \alpha q - 2\tilde{g} - \frac{\lambda_-^2}{4\kappa}$  and the phonon frequency  $\omega_0 = \sqrt{\kappa}$  (for convenience, we have taken the mass  $M = 1$  in Eq.4). The second term is the interaction part

$$\begin{aligned} \delta H_1^{(2)} = & \int dx [\alpha a_1 \cos(qx) u_1' u_2 + D \sin(qx) u_1 u_2 \\ & + \frac{1}{2} \beta (-\lambda_- u_1 \sin(qx) + \lambda_+ u_2)]. \end{aligned} \quad (9)$$

In Eq.9, the terms in the first line couple  $u_1(k)$  with  $u_2(k \pm q)$  and vice versa and modify the gap  $\Delta_0$  between

two magnon modes. In general, as shown in Fig.4, the coupling creates a distinguished kink in dispersion curve around  $k = q/2$  rather than a finite energy jump at  $k = q/2$  which is normally expected in the ICM phase described in a simple Sine-Gordon model[? ]. The terms in the second line describe the coupling between the magnon and the phonon. The coupling results in two general effects. First, the coupling leads to a change of phonon frequency. Under condition  $\omega_0^2 \gg \rho E_i(0)$ , the shift frequency of the phonon is roughly given by  $\delta\omega^2 = \frac{\rho\lambda_+^2}{4(\omega_0^2 - \rho E_2(0))} + \frac{\rho\lambda_-^2}{8(\omega_0^2 - \rho E_2(q))}$ . Second, the coupling allows us to measure the magnons in optical conductivity. The optical conductivity is given by  $\sigma(\omega) = \omega \text{Im}[G_{\beta\beta}(\omega, 0)]$ , where  $G_{\beta\beta}(\omega, k)$  is the full propagator of the  $\beta$ . In our model, we expect double peaks in the optical conductivity at the gap energy of the two magnons in the ICM phase. Up to the second order, we have,  $\text{Im}[G_{\beta\beta}(\omega, 0)] = \pi [\rho \frac{\lambda_-^2}{8\omega_0^4} \delta(\omega^2 - \rho E_1(q)) + \rho \frac{\lambda_+^2}{4\omega_0^4} \delta(\omega^2 - \rho E_2(0)) + (1 - \rho \frac{\lambda_-^2/2 + \lambda_+^2}{4\omega_0^4}) \delta(\omega^2 - \omega_0^2 - \delta\omega^2)]$ . In Fig.4, by numerically solving the dynamical equations of  $\delta H^{(2)}$ , we plot the result of  $\sigma(\omega)$  and the dispersions of electromagnons with a typical parameter setting  $\{\rho, \alpha, \lambda_+, \lambda_-, \kappa, D, g\} = \{2, 0.4, 0.06, 0.06, 2, 0.002, 0.005\}$ .

*Effects of external magnetic field:* In our model, since  $\vec{n}$  is the staggered moment field, the effect of an external magnetic field  $H$  is equivalent to creating an easy plane. However, since the staggered moment is in the a-b plane, the effect of the field is only important when the field is along the a or b axis. In the presence of the easy axis parameter  $D$  along the a axis, the effects of the external magnetic fields along the a axis,  $H_a$ , and b axis,  $H_b$ , have exact opposite effects. They simply change  $D$  to

$$D(H_a, H_b) = D - H_a^2/2\rho + H_b^2/2\rho \quad (10)$$

in Eq.5. From  $E_1(k)$ ,  $E_2(k)$ , Eq.9 and Eq.6, Eq.10 leads to a few important and immediate predictions. First, the effects of  $H_a$  and  $H_b$  do not depend on their directions along their own axis. Second,  $H_b$  can drive the system from the ICM phase to the CM phase while  $H_a$  can drive the system from the CM phase to the ICM phase. This result has been observed experimentally in [? ]. The critical fields to drive the transition can be estimated for the one dimensional system from Eq.6. Third, in the ICM phase, the energy dispersions of the electromagnons as a function of  $H_a$  and  $H_b$  can be predicted. From  $E_1(k)$ ,  $E_2(k)$  and Eq.9, the energy of the electromagnons is expected to increase (decrease) as  $H_b$  ( $H_a$ ) increases. Finally, the external magnetic field does not add additional peaks, which contradicts the conventional picture of the Zeeman energy splitting of magnons.

In conclusion, we develop an effective model that explains the phase diagram and the mechanism of magnetoelectric coupling in multiferroics  $RMn_2O_5$ . To our knowledge, this is the first theoretical effective model for

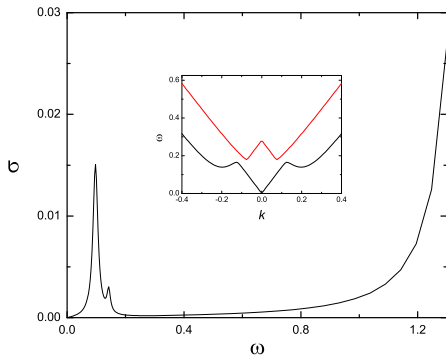


FIG. 4: The numerical result of the optical conductivity versus frequency with the parameters set to:  $\{\rho, \alpha, \lambda_+, \lambda_-, \kappa, D, g\} = \{2, 0.4, 0.06, 0.06, 2, 0.002, 0.005\}$ . The inset is the dispersion of the electromagnons.

these materials. A detailed study of low energy excitations in one dimension is performed to explain the selection rules of electromagnon in optical conductivity measurements[? ]. Our prediction of the electromagnon dispersion and its dependence on the external magnetic field can be tested in future experiments. A quantitative study of our model incorporating the experimental data on different  $RMn_2O_5$  materials will be reported elsewhere[? ]. We expect that the model presented here can be applied to other multiferronics materials where ferroelectricity is correlated to a collinear or col-plane magnetic phase.

*Acknowledgments* J. Hu thanks S. Kivelson and S. Brown for teaching some concepts presented in this paper. We thank A. B. Sushkov, R.V. Aguilar and D. Drew for important comments and extremely useful discussion. We also thank M. Mostovoy for useful discussion in APS March meeting (2007). This work was supported by the National Science Foundation under grant number PHY-0603759.